Evaluation of SARS-COV-2 transmission and infection in airliner cabins

Wensi Wang[1], Feng Wang[1], Dayi Lai[2*] and Qingyan Chen[3]

[1]Tianjin Key Laboratory of Indoor Air Environmental Quality Control, School of Environmental Science and Engineering, Tianjin University, 92 Weijin Road, Tianjin, 300072, China
[2]Department of Architecture, Shanghai Jiao Tong University, Shanghai 200240, China
[3] Department of Building Environment and Energy Engineering, The Hong Kong Polytechnic University, Kowloon, Hong Kong

[*]*Corresponding email: dayi_lai@sjtu.edu.cn*

Abstract

Commercial airliners have played an important role in spreading the SARS-CoV-2 virus worldwide. This study used computational fluid dynamics (CFD) to simulate the transmission of SARS-CoV-2 on a flight from London to Hanoi and another from Singapore to Hangzhou. The dispersion of droplets of different sizes generated by coughing, talking, and breathing activities in a cabin by an infected person was simulated by means of the Lagrangian method. The SARS-CoV-2 virus contained in expiratory droplets traveled with the cabin air distribution and was inhaled by other passengers. Infection was determined by counting the number of viral copies inhaled by each passenger. According to the results, our method correctly predicted 84% of the infected/uninfected cases on the first flight. The results also show that wearing masks and reducing conversation frequency between passengers could help to reduce the risk of exposure on the second flight.

Keywords: COVID-19; Airborne diseases; Exhaled droplets; Air distribution; Risk assessment.

Practical Implications

By simulating the SARS-CoV-2 transmission via coughing, breathing, and talking for two real flights, our paper reveals that 99% of the inhaled virus copies are carried by droplet nuclei smaller 10 μm in aircraft cabin. This study also confirmed the positive effect of using masks and limiting conversation frequency. These findings are useful for reducing onboard transmission of SARS-CoV-2.

1. Introduction

The global spread of COVID-19 caused about five million deaths by October 2021 [1]. The virus spread rapidly to various countries and continents [2], and long-distance commercial airliners played an important role. For example, early flights from London to Hanoi [3], from Boston to Hong Kong [4], and from Dubai to New Zealand [5] spread SARS-CoV-2 on a global scale. Although there have been numerous cases of infection on airplanes, the majority of flights have not spread the disease. To reduce the risk of SARS-CoV-2 transmission during air travel, it is necessary to understand the transmission of the virus in airliner cabins.

SARS-CoV-2 is transmitted through droplets generated by an infected person's exhalation activities (breathing, coughing, talking, and sneezing) [6]. Therefore, the transmission of droplets in airliner cabins must be studied. Such an investigation would require the thermo-fluid boundary conditions of the exhaled droplets, such as the expiratory velocity [7–10] and temperature [11], droplet composition [12], and droplet size distribution [13–18]. Because the dispersion of exhaled droplets is determined predominately by the droplet diameter and their interactions with the local airflow [19], the droplet size distribution is a key factor. The droplets from a person's exhalation activities range widely in size, from 0.1 μm to 2000 μm [13–18]. Large droplets are influenced primarily by inertial force and gravity, and can travel from the patient's nose or mouth to susceptible mucosal (mouth, nose) or conjunctival (eyes) surfaces of a nearby person. Small droplets (airborne) can remain suspended in the air for a long time [19] and can be inhaled by fellow passengers. Therefore, thorough analysis of droplet transmission and assessment of the infection risk for susceptible passengers in aircraft cabins require the full size range of exhaled droplets.

Many studies have utilized the full range of droplet sizes for understanding the transmission of exhaled droplets, but these studies have rarely assessed the infection risk in indoor environments. For example, Yan et al. [19] studied the effect of a human thermal plume on the evaporation and diffusion of cough droplets with diameters of 3 μm to 750 μm, and found that the thermal plume from the human body was a key parameter not only in droplet evaporation, but also in droplet deposition time, increasing the transmission distance of droplets. Feng et al. [20] studied the influence of wind and relative humidity on the spread of cough droplets with diameters of 2 μm to 2000 μm, and found that airflow had a very important influence on the spread of small droplets, while high relative humidity made large droplets easy to deposit. Yan et al. [21] studied the impact of a cough jet on the travel of particles with diameters of 2 μm to 1000 μm in a three-row Boeing 737 model, and found that the cough jet had a considerable effect on large droplets. However, their research used only one or two

manikins, and thus the scenario was different from a high-density aircraft cabin. Talaat et al. [22] investigated the diffusion of exhaled particles with diameters of 1 μm to 50 μm for different passenger capacities, with/without sneeze guards/shields between passengers, in a ten-row Boeing 737 model. They found that the guards were more economically attractive than reducing passenger capacity by vacating middle seats. Although their study provided useful information for preventing droplet transmission in a cabin, it did not include droplets with sizes less than 1 μm in diameter, which account for quite significant portions of the droplets exhaled in breathing and coughing [13,14,16] and of those that carry viruses [23]. Therefore, it is necessary to include droplets smaller than 1 μm when studying droplet transmission.

Apart from the droplet transmission studies, many investigations of infection risk have used mono-dispersed particles or a gas to represent an exhalation activity. Gupta et al. [24,25] utilized particles with sizes of 0.4 μm, 8.5 μm, and 30 μm to represent the droplets exhaled by coughing, breathing, and talking, and thoroughly explained the use of the deterministic and probabilistic equation to evaluate the infection risk for passengers in a seven-row cabin. Based on the work of Gupta et al. [24,25], Yan et al. [26] used particles with a size of 3.5 μm to represent the droplets exhaled by coughing; they analyzed the droplet transmission and then assessed the risk for passengers in a cabin. Although they made a great effort to assess the risk of airborne diseases in the cabin, they ignored the diversity of droplet sizes in the dispersion. Other researchers [27,28] found that the horizontal travel distance of droplets is related to their size: large droplets (larger than 100 μm) settle within 2 m, medium-sized droplets can travel up to 4 m, and small droplets (smaller than 10 μm) can travel farther. Due to the high passenger density in economy-class aircraft cabins, larger droplets may reach neighboring passengers. Hence, using small mono-dispersed particles or gas to represent an exhalation activity would result in underestimation of the risk to susceptible passengers posed by neighboring index passengers, and overestimation of the risk to susceptible passengers seated far away from index passengers. The use of large droplets would give rise to the reverse situation. Therefore, the full spectrum of droplet sizes are required for assessing the infection risk for passengers in aircraft cabins.

To comprehensively investigate the transmission and infection processes for SARS-COV-2 in airliner cabins, this investigation sought to develop a method that included the full size spectrum of virus-laden droplets generated by coughing, breathing, and talking activities. The method would provide an accurate assessment of infection risk. Our study used two actual long-distance flights with SARS-COV-2 transmission and infection as examples to demonstrate the validity of the research method.

2. Methods

2.1 Simulation of SARS-CoV-2 transmission in an aircraft cabin

The two main approaches for studying droplet transmission in an aircraft cabin are experimental measurements and computer simulations. Experimental measurements can provide realistic and reliable information [29–31], but it can be prohibitively expensive to build mockups that represent various aircraft models and to reproduce the distribution of full-size particles. Compared with experimental methods, computational fluid dynamics (CFD) simulations are inexpensive, and aircraft cabin models and boundary conditions can easily be changed in CFD. Therefore, this investigation used CFD to study the transmission of SARS-COV-2 in airliner cabins.

Because the RNG k-ε model performs well in predicting mixed convection airflow in enclosed spaces [32], this study used the model in the commercial CFD software ANSYS Fluent [33] to predict turbulent flow in cabins. The RNG k-ε model solved the following governing equation:

$$\frac{\partial(\rho\Phi)}{\partial t} + div\left(\rho\vec{u}\Phi - \Gamma_{\varphi,eff} grad(\Phi)\right) = S_{\Phi} \quad (1)$$

where Φ represents the time-averaged velocity components $\overrightarrow{u_i}$ $(i = 1, 2, 3)$, turbulent kinetic energy k, rate of dissipation of turbulent kinetic energy ε, and enthalpy H, ρ is air densityWhen Φ is unity, the equation represents the conservation of mass. The t is time, $\vec{u}$ is the Reynolds-averaged air velocity vector, $\Gamma_{\varphi,eff}$ is a coefficient, and S_{Φ} is the source. Details of the RNG k-ε model can be found in the FLUENT guide [33].

After solving the flow field, we studied the particle dispersion in the cabin. The transport of particles can be predicted by either the Eulerian or the Lagrangian method. Of the two methods, the Lagrangian performs better in predicting the transient dispersion of particles [34]. Therefore, the Lagrangian method was used to track the particle movement based on Newton's second law. Significant forces including the gravity $\overrightarrow{F_G}$ and the drag force $\overrightarrow{F_D}$ were considered through the following equations [35]:

$$m_d \frac{\overrightarrow{du_d}}{dt} = \overrightarrow{F_G} + \overrightarrow{F_D} \quad (2)$$

$$\overrightarrow{F_G} = \frac{\pi d_d^3}{6}(\rho_d - \rho) \quad (3)$$

$$\overrightarrow{F_D} = \frac{C_D}{2}\frac{\pi d_d^2}{4}\rho|\overrightarrow{u_d} - \vec{u}|(\overrightarrow{u_d} - \vec{u})/C_c \quad (4)$$

where d_p is droplet diameter, ρ_d droplet density, $\overrightarrow{u_p}$ droplet velocity, $\vec{u}$ the fluid phase velocity, C_c the Cunningham correction factor [36], and C_D the drag coefficient. The C_D is expressed as:

$$C_D = a_1 + \frac{a_2}{Re_d} + \frac{a_3}{Re_d^2} \quad (5)$$

where a_1, a_2, a_3 are coefficients. They are determined by the droplet Reynolds number [37]:

$$Re_d = \frac{|\overrightarrow{u_d} - \vec{u}|d_p}{\upsilon} \quad (6)$$

where υ is kinematic viscosity.

Because the volume fraction of expiratory droplets is low, one-way coupling was used. Only the fluid flow has an influence on the dispersed phase (particles), and the effect of the dispersed phase on the fluid flow was neglected. However, because the RNG k-ε model calculates the Reynolds time-averaged velocity, and not the fluctuating flow velocity, the discrete random walk (DRW) model was used to simulate the interaction of a particle with a succession of discrete stylized fluid-phase turbulent eddies.

This study solved the above equations by using the commercial CFD program FLUENT. Table 1 provides the boundary conditions used to calculate the air distribution in a cabin. To reduce the error caused by the mesh, grid-independence tests were conducted.

Table 1. Boundary conditions for calculating cabin air distribution.

Boundary	Velocity (m/s)	Temperature (K)
Inlet	1.73	292.85
Ceiling	No slip	295.65
Luggage	No slip	295.35
High wall	No slip	295.25
Low wall	No slip	295.15
Floor	No slip	294.85
Head	No slip	304.65
Body	No slip	298.15

Seat	No slip	295.95
Mouth		307 [11]
Nose		306 [11]
Display screen (VN54)	No slip	301.65
Lavatory outlet (TR188)	21.5 m^3/h each	

170

171 **2.2 Source information**

172 To accurately assess the infection risk of COVID-19, it is essential to provide the
173 correct source information in the CFD model. A COVID-19 patient could generate the
174 SARS-CoV-2 virus through the exhalation of respiratory droplets. It should be noted
175 that there are two types of index patients, symptomatic and asymptomatic.
176 Symptomatic patients produce infectious droplets through breathing, talking, and
177 coughing, without sneezing [38]. Since asymptomatic patients do not cough, they
178 generate virus-laden droplets only through breathing and talking. The coughing
179 frequency was set to 25 times/h for seated passengers and 15 times/h for reclining
180 passengers. The breathing frequency was 720 times/h, while for talking, two people
181 talked alternately with each person speaking for 10 s in turn [8,9].

182 The sizes of droplets generated by human breathing, coughing, and talking varied
183 in a wide range. Figure 1 shows the size spectrum of droplets for different activities
184 from the literature. Fabian et al. [13] recommended using particles with diameters of
185 0.4 μm, 0.75 μm, and 2.5 μm as shown in Figure 1(a). Figure 1(b) illustrates the size
186 range of cough-generated droplets from Chao et al. [15] and Yang et al. [14]. The
187 present investigation used data measured by Chao et al. [15] as shown in Figure 1(c).

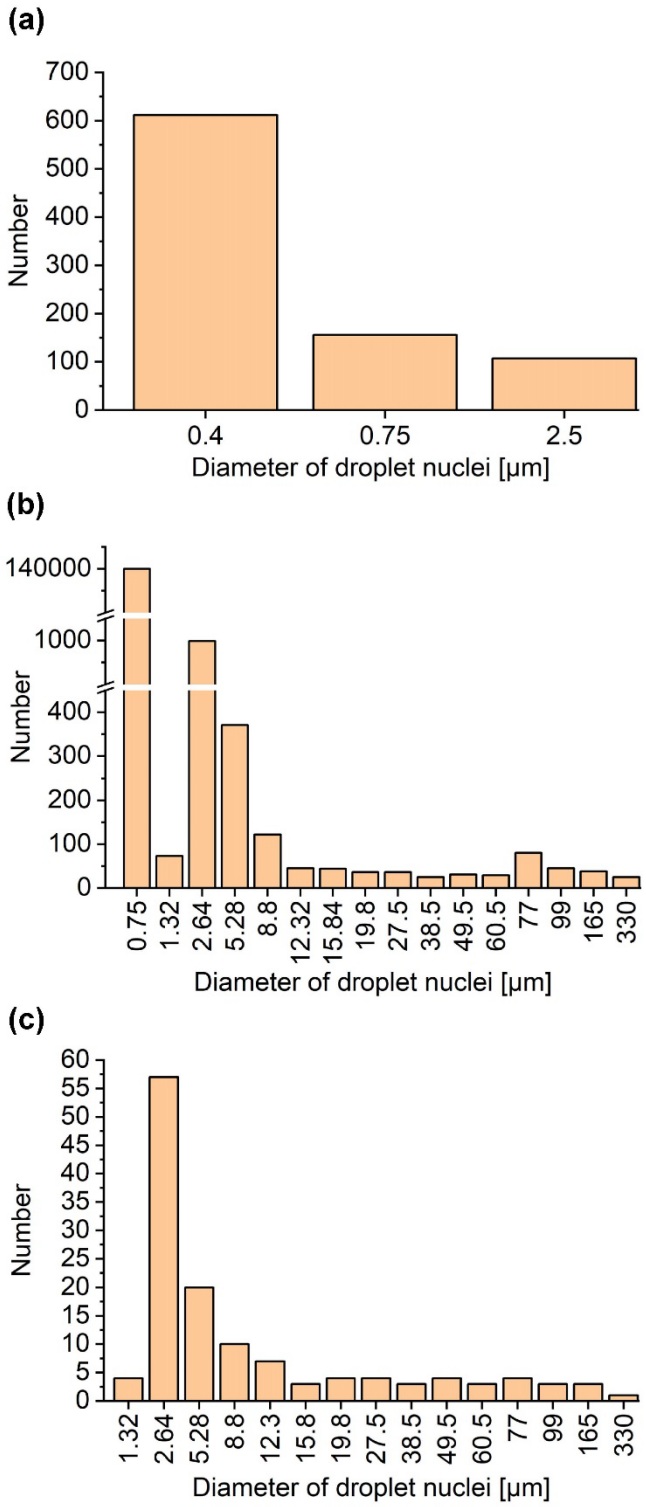

Figure 1. Droplet size and number generated by: (a) a single breath, (b) a single cough, and (c) one second of talking.

The SARS-CoV-2 virus load in the droplets is also an important factor. The virus load in a single droplet with diameter d, v_d, can be calculated by:

$$v_d = C_d \times V_d \tag{7}$$

where C_d and V_d are the virus concentration (copies/ml) and volume (ml), respectively, of a droplet with diameter d. According to Johnson et al. [39], droplets with a diameter greater than 20 μm come from the mouth, while those smaller than 20 μm come from the respiratory tract. Pan et al. [40] and To et al. [41] measured the virus concentrations in saliva and sputum as 1.2×10^8 copies/mL and 1.34×10^{11} copies/mL, respectively. With the common knowledge that saliva comes from mouth and sputum from the respiratory tract, the droplets with diameters greater than 20 μm had a virus concentration of 1.2×10^8 copies/mL and those smaller than 20 μm had a concentration of 1.34×10^{11} copies/mL.

For coughing and talking, the virus concentration C_d for droplets smaller than 20 μm was further calibrated according to data from Lindsley et al. [42]. Their measurements [42] demonstrated that the 35%, 23%, and 42% of the detected influenza RNA was contained in cough-generated droplets with particle size ranges of > 4 μm, 1–4 μm, and < 1 μm, respectively. In this study we used viral content distribution from influenza instead of SARS-CoV-2 because there was no detailed data on the SARS-CoV-2 viral load of droplets emitted by COVID-19 patients. The droplets of various respiratory infections showed similarities in aerosol size distributions, with a predominance of pathogens in small particles (<5 μm) [43]. We used the same method to calibrate the virus concentration for talking. We could then calculate the viral load in different droplets as shown in Tables 2 through 4 for breathing, coughing, and talking, respectively.

Table 2. Number of viral copies in droplet nucleus from breathing.

Diameter [μm]	Copies [/droplet]
0.4	0.0045
0.75	0.0294
2.5	1.0904

Table 3. Number of viral copies in droplet nucleus from coughing.

Diameter [μm]	Copies [/droplet]
0.75	0.43
1.32	5
2.64	41
5.28	80
8.8	370
12.3	1

15.8	3
19.8	6
27.5	15
38.5	42
49.5	89
60.5	163
77.0	337
99.0	716
165.0	3313
330.0	26507

Table 4. Number of viral copies in droplet nucleus from talking

Diameter [μm]	Copies [/droplet]
1.32	7
2.64	55
5.28	87
8.8	402
12.3	1
15.8	3
19.8	6
27.5	15
38.5	42
49.5	89
60.5	163
77.0	337
99.0	716
165.0	3313
330.0	26507

In addition to viral load, the source thermo-fluid conditions play an important role in virus transmission in an aircraft cabin. Figure 2(a) depicts the velocity of a cough jet [8,9] for a person without a mask. For a person with a mask, this study used a method from Chen et al. [10] to decompose the velocity of a cough into upward and forward directions, as shown in Figure 2(b). Breath velocity is a sine wave function according to Gupta et al. [8,9], as displayed in Figure 2(c). A talking person produces outward

velocity through the mouth, but takes in air through the nose. When the talking stops, the velocity returns to the normal breath boundary [8,9]. Figure 2(d) shows the flow rate for two passengers having a 10 s conversation in which they take turns speaking.

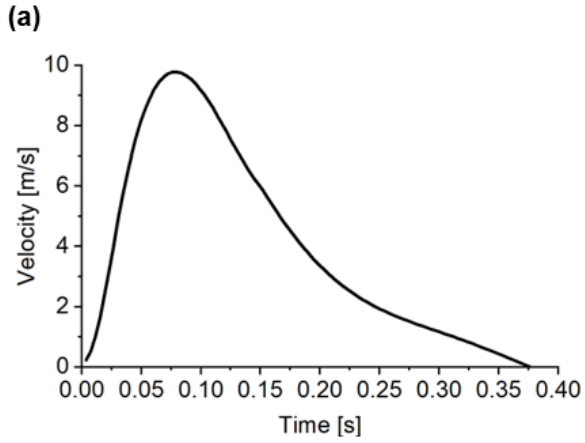

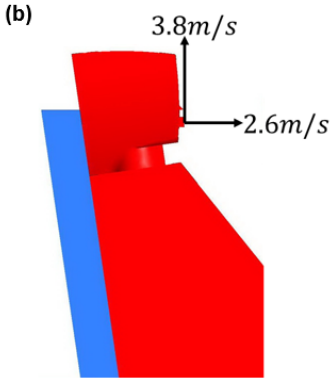

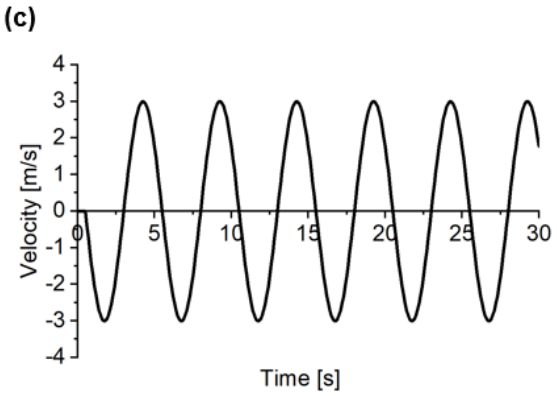

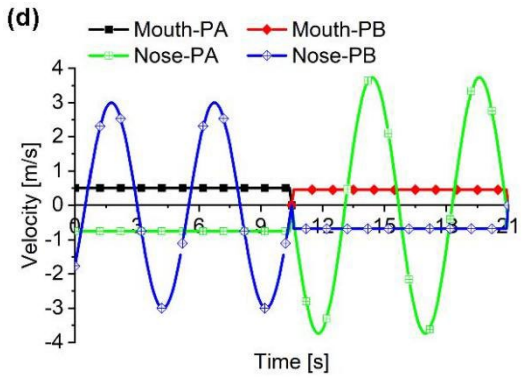

Figure 2. Flow boundary conditions for the index passenger for (a) coughing without a mask, (b) coughing with a mask, (c) breathing, and (d) talking between two passengers.

2.3 Inhalation of virus-laden droplets

The virus-laden droplets in a cabin are inhaled by passengers. If a passenger is wearing a mask, it acts as a filter to capture expiratory droplets and inhalation droplets. After being filtered by the mask (or not), the droplets enter the respiratory system; they may be deposited in the respiratory system or exhaled. Under the assumption that surgical masks are worn during flights, droplets greater than 5.28 μm in diameter would all captured by a passenger's mask and deposited in the respiratory system. A fraction of droplets with sizes smaller than 5.28 μm might pass through the surgical mask and deposit in the respiratory system, with a filter efficiency and deposition fraction as shown in Table 5.

Table 5 Filter efficiency of a surgical mask for breathing in and out, and total deposition fraction in the respiratory tract.

Diameter [μm]	Inward filtration efficiency [44]	Outward filtration efficiency [44]	Deposition fraction [45]
0.75	33.4%	67.3%	44.0%
1.32	39.5%	73.0%	58.0%
2.64	45.4%	78.0%	75.0%
5.28	89.0%	93.0%	82.0%

Using the Lagrangian method to predict all activities throughout an entire flight would require too much time and usage of computing resources. This investigation used a semi-analytical method and a superposition method [46] with CFD simulations to determine the total number of inhaled droplets. The semi-analytical method assumes perfect mixing [46,47] of droplets within 240 s from their release into the air. The

concentration of droplets with diameter d $C_d(t)$ at time t (in seconds) at any point in the cabin can be calculated as:

$$C_d(t) = \frac{N_d(240)exp(-Q(t-240)/V)}{V} \quad (8)$$

where $N_d(240)$ is the number of droplets with diameter d in the cabin at 240 s, Q is the ventilation rate of the cabin (m^3/s), and V is the volume of the cabin (m^3). The number of droplets inhaled per second with diameter d, $n_d(t)$, at time t ($t > 240$ s), can be written as:

$$n_d(t) = pC_d(t) \quad (9)$$

where p is the passenger's inhalation rate, m^3/s. Before t = 240 s, $n_d(t)$ was calculated by the Lagrangian method.

The number of viral copies inhaled by a passenger from a single activity (coughing, breathing, or talking), $nv(t)$, can be determined as:

$$nv(t) = \sum_{for\ all\ d} n_d(t) \times v_d \times P_d \quad (10)$$

The total penetration fraction of droplets with diameter d can be expressed as:

$$P_d = f_{rt,d} \times (1 - f_{m-in,d}) \times (1 - f_{m-out,d}) \quad (11)$$

where $f_{rt,d}$, $f_{m-in,d}$, and $f_{m-out,d}$ are the deposition fractions of particles with diameter d in the respiratory tract, and the inward and outward filter efficiency of the mask for droplets with a diameter of d, respectively.

With the superposition method from Gupta [46], the number of inhaled virus copies for combined breathing, coughing, and talking at time t, $nv_{all}(t)$ is:

$$nv_{all}(t) = \sum_{for\ all\ m} nv_c(t - t_m) + \sum_{for\ all\ j} nv_b(t - t_j) + \sum_{for\ all\ k} nv_t(t - t_k) \quad (12)$$

where $nv_c(t - t_m)$ is the number of inhaled viral copies at time $(t - t_m)$ for coughing at t_m; $nv_b(t - t_j)$ is the number of inhaled viral copies at time $(t - t_j)$ for breathing at t_j; and $nv_t(t - t_k)$ is the number of inhaled viral copies at time $(t - t_k)$ for taking

303 at t_k.
304 Equation (12) can be used to calculate the number of viral copies inhaled by a passenger
305 during a flight. If a passenger inhaled 2000 copies of SARS-COV-2, the passenger
306 would be infected [48].
307

308 **3. Validation of CFD model**

309 Among the various research methods, CFD modeling is crucial but entails a high
310 uncertainty due to the approximations used. Therefore, it is necessary to validate the
311 CFD simulation results. Experimental data from Li et al. [30] in a single-aisle aircraft
312 cabin were used for validation in the present study. The data includes distributions of
313 airflow, air temperature, and particle concentration.
314 Figure 3(a) compares the measured and simulated air patterns in a cross section of
315 the cabin. The results show that air from the side supply and the ceiling supply formed
316 two large vortices above the seats, and was then exhausted at the bottom of the cabin.
317 However, because the RNG k-ε model underpredicted the turbulence energy [49], the
318 decay of the simulated velocity was slower than that in the experiment; as a result the
319 simulated velocity was greater than the experimental value in the aisle.
320 Figure 3(b) compares the simulated and measured air temperature distributions.
321 Since the air in the cross section was well mixed, the air temperature distribution was
322 relatively uniform. However, a difference can be seen in the mid-cabin region. Due to
323 the slow attenuation of velocity in the simulation, the simulated temperature was lower
324 than that in the experiment. In general, since the difference between the predicted and
325 measured results was less than 1 K, and the measurement accuracy was $\pm$0.5 K [50],
326 the temperature field was predicted with reasonably good accuracy.
327 To verify the accuracy of the Lagrangian method in calculating the particle
328 dispersion, this investigation used the method to simulate the dispersion of 1 μm
329 particles in accordance with the experimental settings of Li et al. [30]. Those
330 researchers [30] had calculated the dimensionless particle concentration, C*, by:
331

332 $$C^* = \frac{C_{local} - C_{in}}{C_{out} - C_{in}} \quad (13)$$

333

334 where C_{local} is the particle number concentration at a sampling point, $particles/cm^3$;
335 C_{in} is the particle number concentration in the air supply; and C_{out} is the nominal
336 exhaust particle concentration without considering particle transmission loss,
337 $particles/cm^3$. Figure 3(c) compares the measured and predicted particle distributions.
338 Because two vortices formed in opposite directions on the left and right sides, separated

by downward airflow in the middle, the particles were confined to the right side of the cabin. The CFD results agreed well with the measurement data.

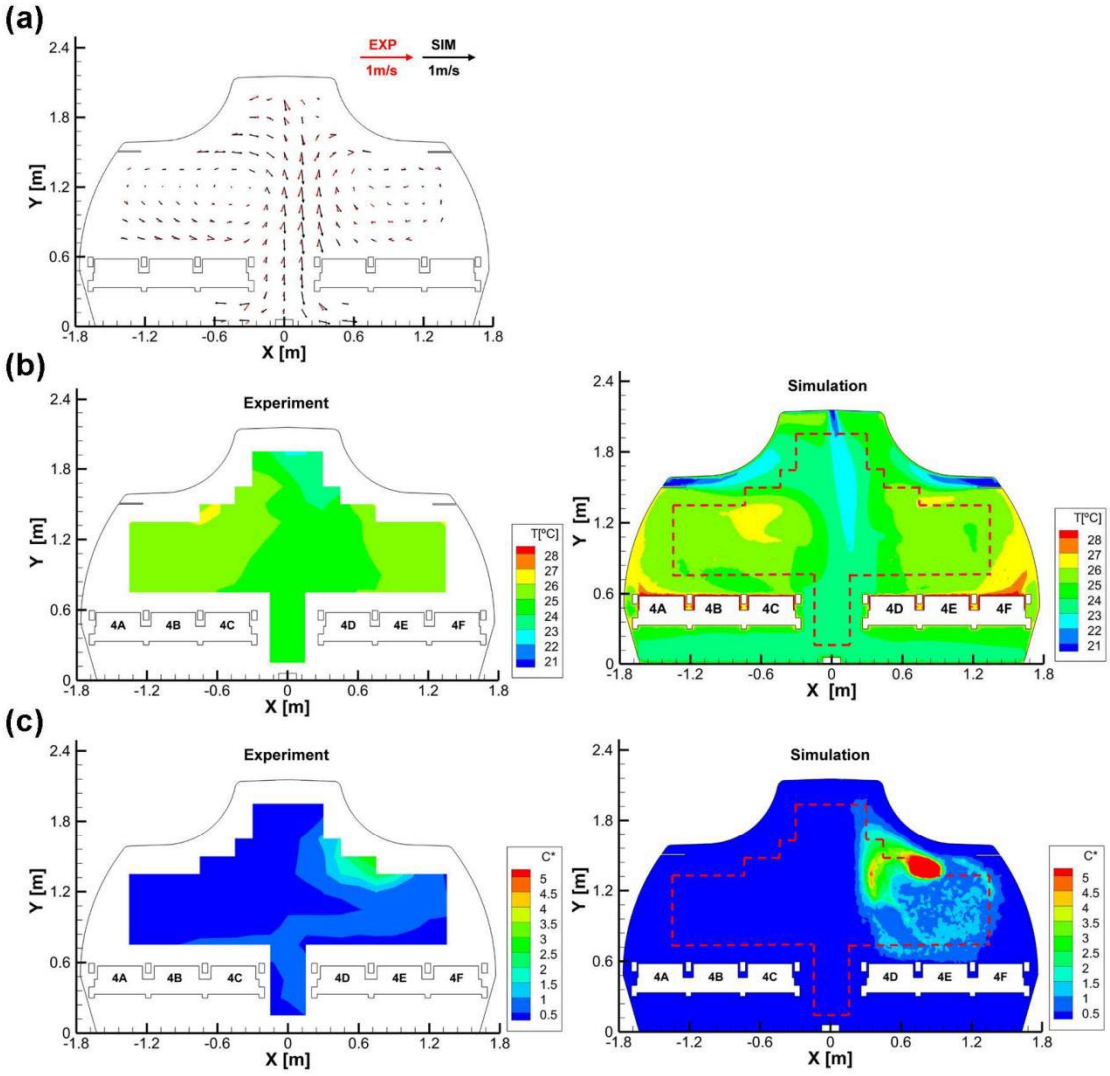

Figure 3. Comparison between the measured and predicted (a) airflow fields, (b) temperature distributions, and (c) particle concentrations in the cross section across Row 4.

The above comparisons demonstrate that the CFD simulations can predict the airflow, temperature, and particle dispersion in the cabin mockup reasonably well. Therefore, CFD can be used as a tool to analyze the transmission of exhaled droplets in an aircraft cabin.

4. Results

Using the method described above, this investigation assessed the infection risk for two actual flights with very different COVID-19 infection conditions. The first was

flight VN54 [3], during which one index patient infected 12 fellow passengers in a business-class cabin with a total of 21 passengers. The second was flight TR188 [51], during which only one passenger was confirmed to be infected by 4 index patients around the infected passenger. This section reports the calculated results.

4.1. SARS-CoV-2 transmission during flight VN54

The first studied flight, VN54, departed from London, UK, at 11:10 a.m. (London time, UTC+1) on March 1, 2020, and landed in Hanoi at 5:20 a.m. (Hanoi time, UTC+7) on March 2, 2020. The entire flight duration was 11 hours 50 minutes, including the boarding, taxiing, and flying times. An epidemiological investigation indicated widespread transmission of COVID-19 in the business-class cabin, where 12 of the 21 passengers were infected with COVID-19 via one index patient [3]. Figure 4(a) shows the distribution of COVID-19 infections in the business-class cabin of flight VN54. Passenger 5K was the index patient. As mentioned, a total of 12 passengers were diagnosed with COVID-19, and 7 passengers were confirmed not to be infected. It should be noted that passenger 2A was not tracked. Our study focused on the business-class cabin because the infection on flight VN54 occurred mainly in this location.

Flight VN54 was on a twin-aisle, widebody Boeing 787-9 aircraft, with seven rows in the business-class cabin. As shown in Figure 4(b), this study modeled the entire business-class cabin. Since this was a long-duration intercontinental flight, we assumed that the passengers were sleeping in a reclining position with little talking. Because the flight occurred in an early stage of the pandemic, we assumed no use of face masks, especially for travelers from Europe [52–54].

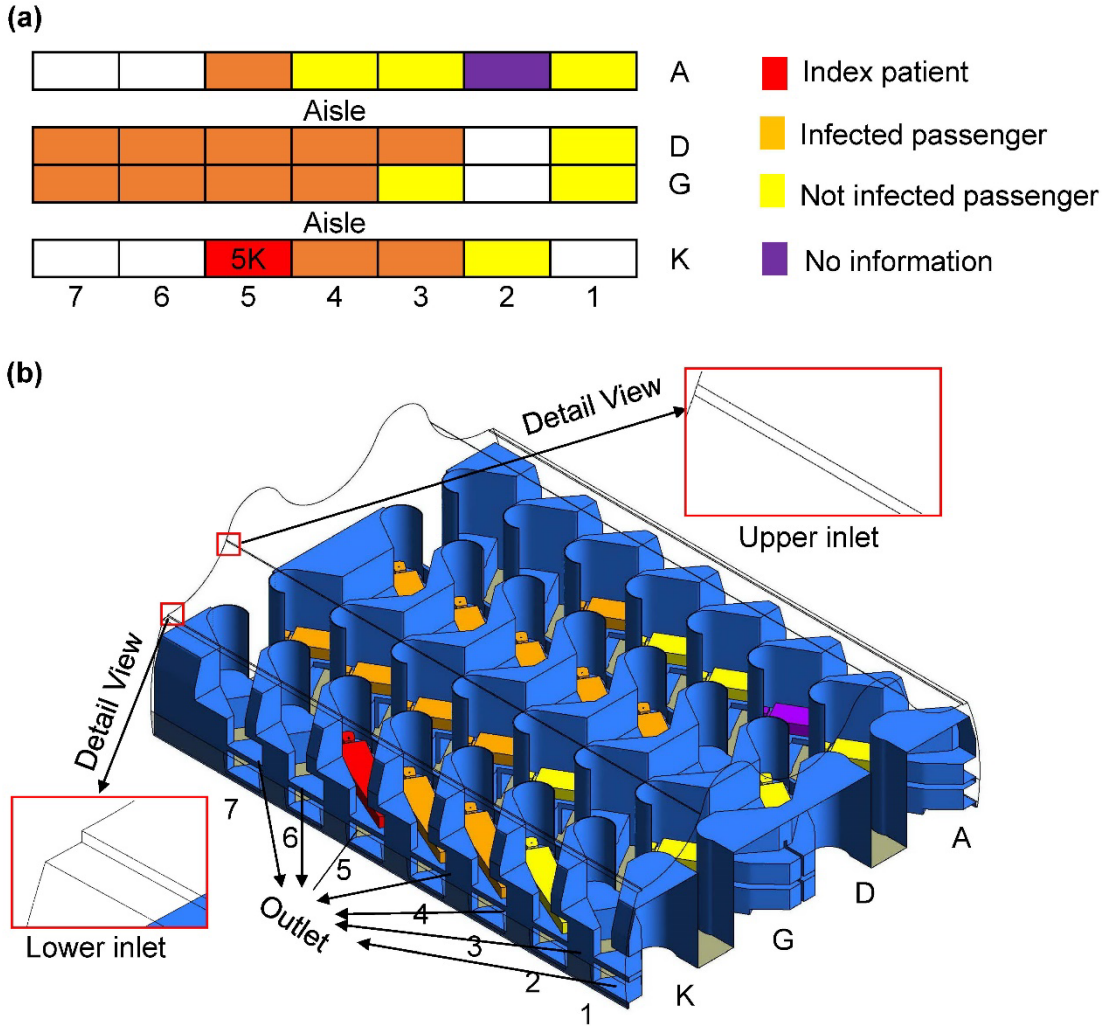

Figure 4. (a) Distribution of COVID-19 infections in the business-class cabin of flight VN54 and (b) geometric model of the Boeing 787-9 business-class cabin.

4.1.1 Airflow

Figure 5(a) depicts the cross-sectional steady-state airflow field, which was used as the initial condition for calculating the transient transport of droplets exhaled during the coughing and breathing of the index patient. The supply air from the side walls and ceiling of the cabin flowed along the walls and collided in the middle of the cabin to form two large-scale circulations. Finally, the recirculated air left the cabin through the outlets near the floor. As shown in Figure 5(b), near vicinity of the passengers produced thermal plumes around the human bodies, and the air velocities around these passengers ranged from 0.2 to 0.3 m/s.

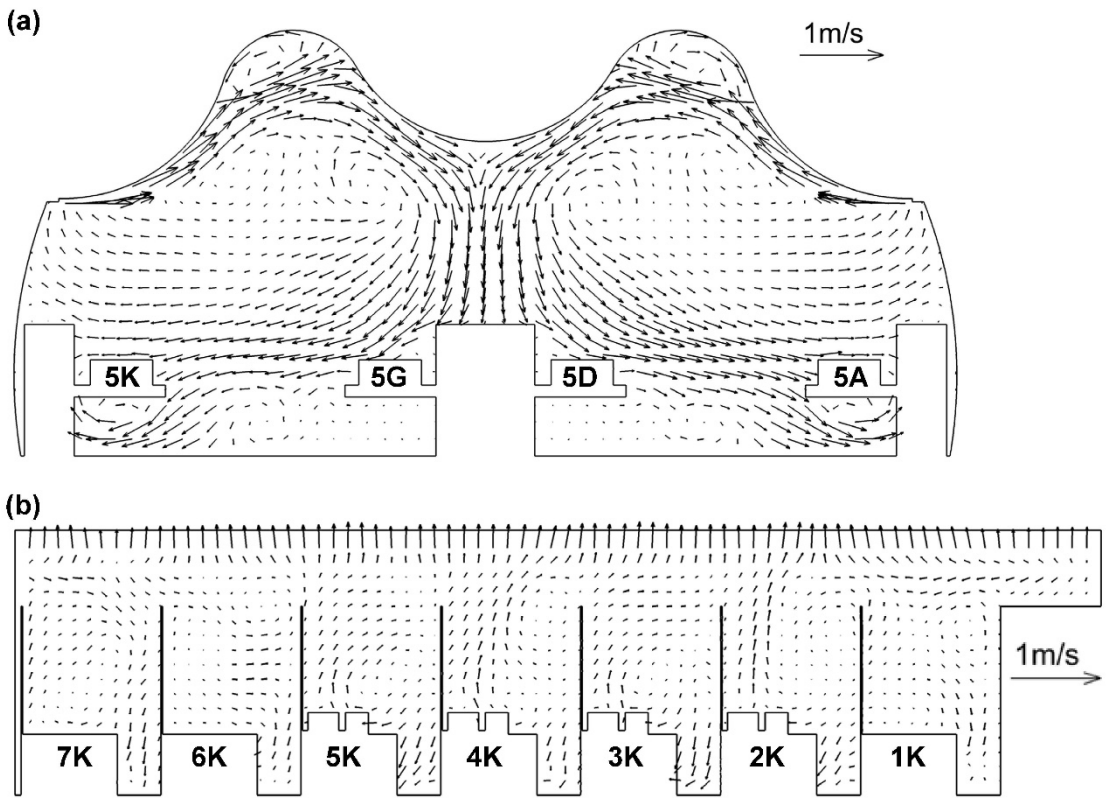

Figure 5. Velocity fields in the cabin on (a) cross-section through the index passenger (b) longitudinal section through the index passenger.

4.1.2 Particle transport

Figure 6 shows the temporal distributions of 1950 droplet nuclei. with sizes ranging from 1 μm to 330 μm, exhaled by a single cough of the index patient. Since the index passenger was reclining, the droplet jets traveled primarily in a vertical direction for the first 10 seconds. Affected by airflow and particle size, droplet nuclei larger than 50 μm deposited near the index passenger's seat due to the large inertial force, while smaller droplets followed the airflow. Due to the collision and mixing of the airflow in the middle, a large portion of the droplets had already spread to the other aisle at 20 s. The particles had diffused to the three rows in front of, and the three rows behind, the index person at 60 s, and were almost perfectly mixed at 240 s. The particle concentration in the cabin decreased with time because the particles were either exhausted by the ventilation system or inhaled by other passengers. Since the particle diffusion mechanism and path were similar between coughing and breathing, the particle transport analysis was not repeated for breathing activity.

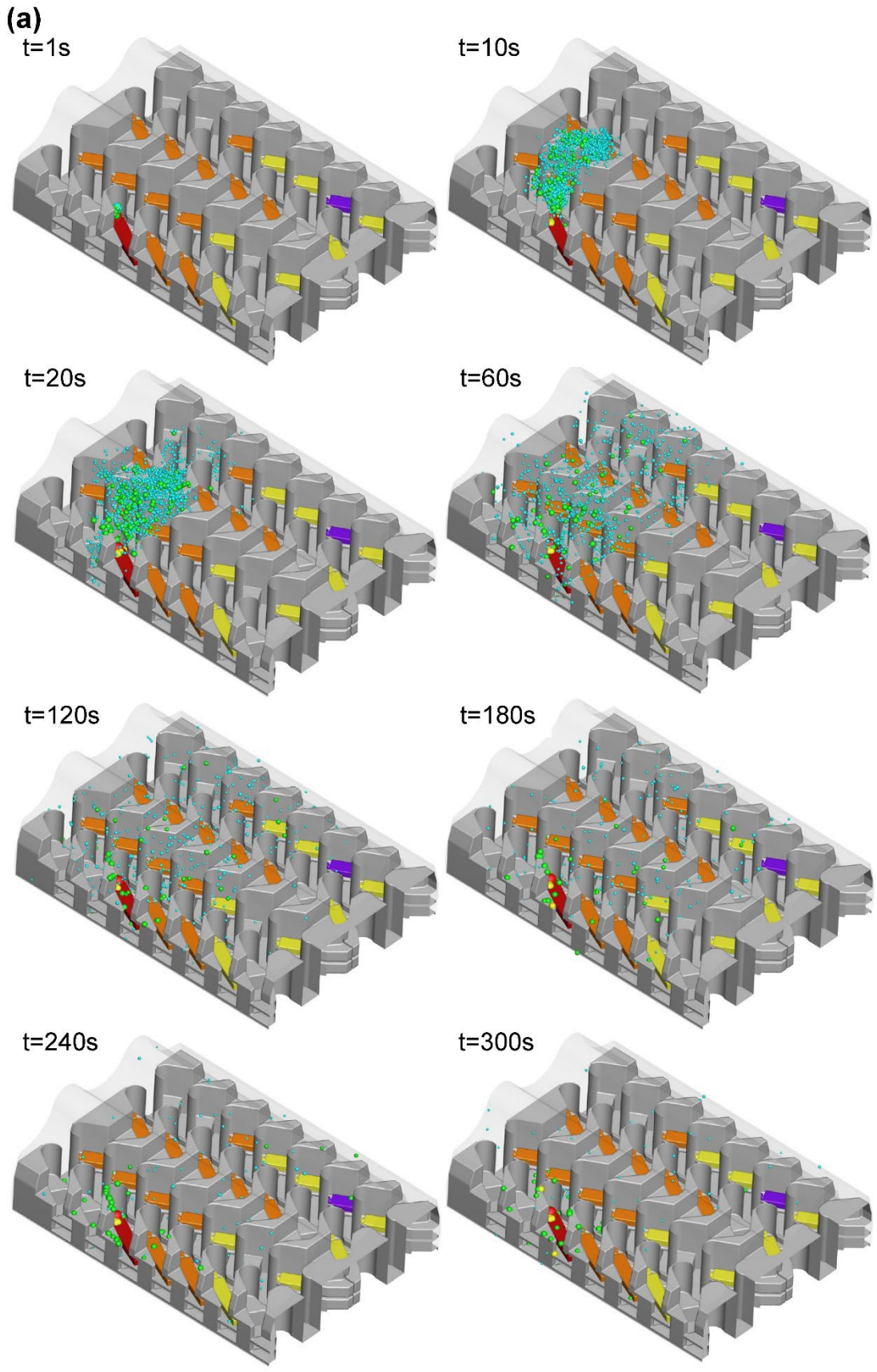

410

411

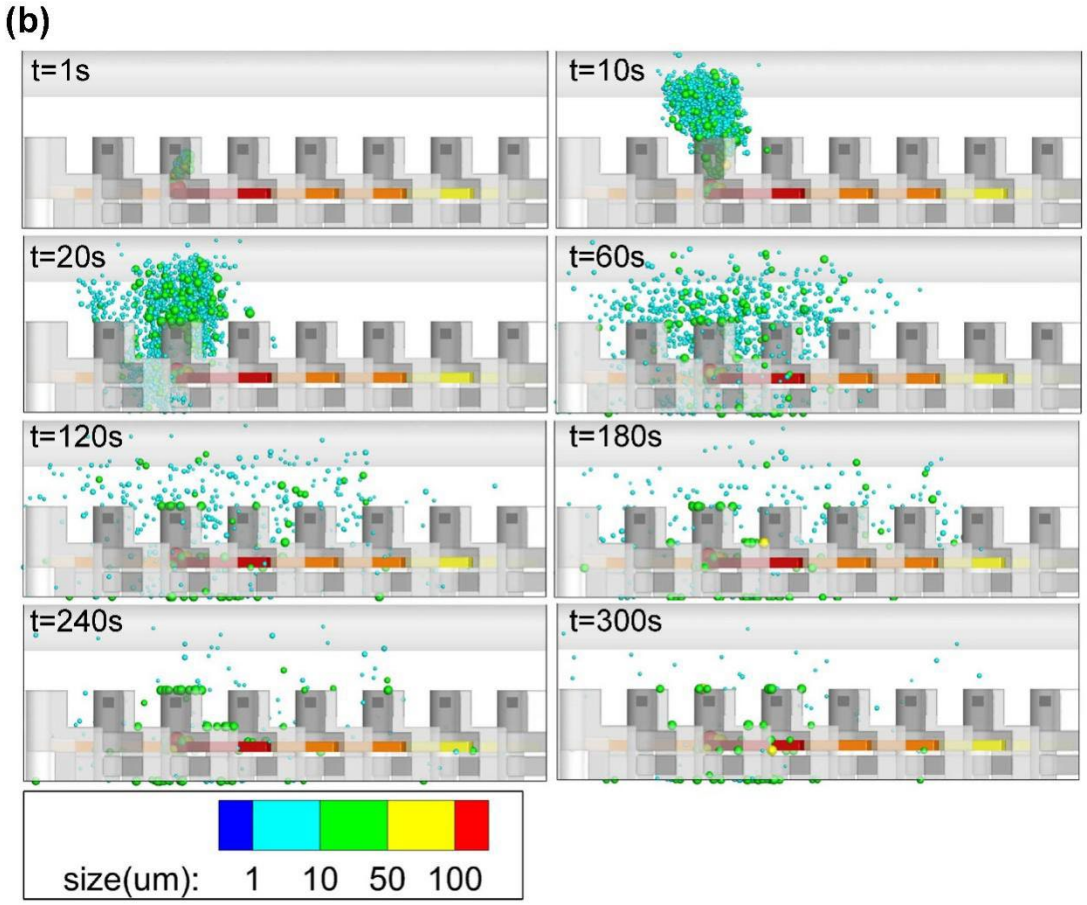

Figure 6. Temporal distributions of droplet nuclei from a single cough in (a) perspective view, and (b) side view in the VN54 case.

4.1.3 Infection risk assessment

The number of viral copies inhaled by each passenger was estimated, as shown in Figure 7(a). Closer proximity to the index patient resulted in greater exposure. The number of viral copies inhaled by the passengers in seats 5G, 6D, and 6G approached or even exceeded 10,000. The infection of fellow passengers can be determined by comparing the number of inhaled viral copies with the tolerance limit of 2000 [48]. The simulated and actual infections are compared in Figure 7(b). The simulation correctly identified 11 of the 12 infected passengers, for an accuracy of 91.7%. Meanwhile, 5 of the 7 uninfected passengers were correctly predicted, for an accuracy of 71.4%. Thus, the calculation successfully predicted the infection condition of 16 of the 19 passengers, for an overall accuracy of 84.2%. It is also worth noting that the infection occurred only two rows in front of and two rows behind the index patient.

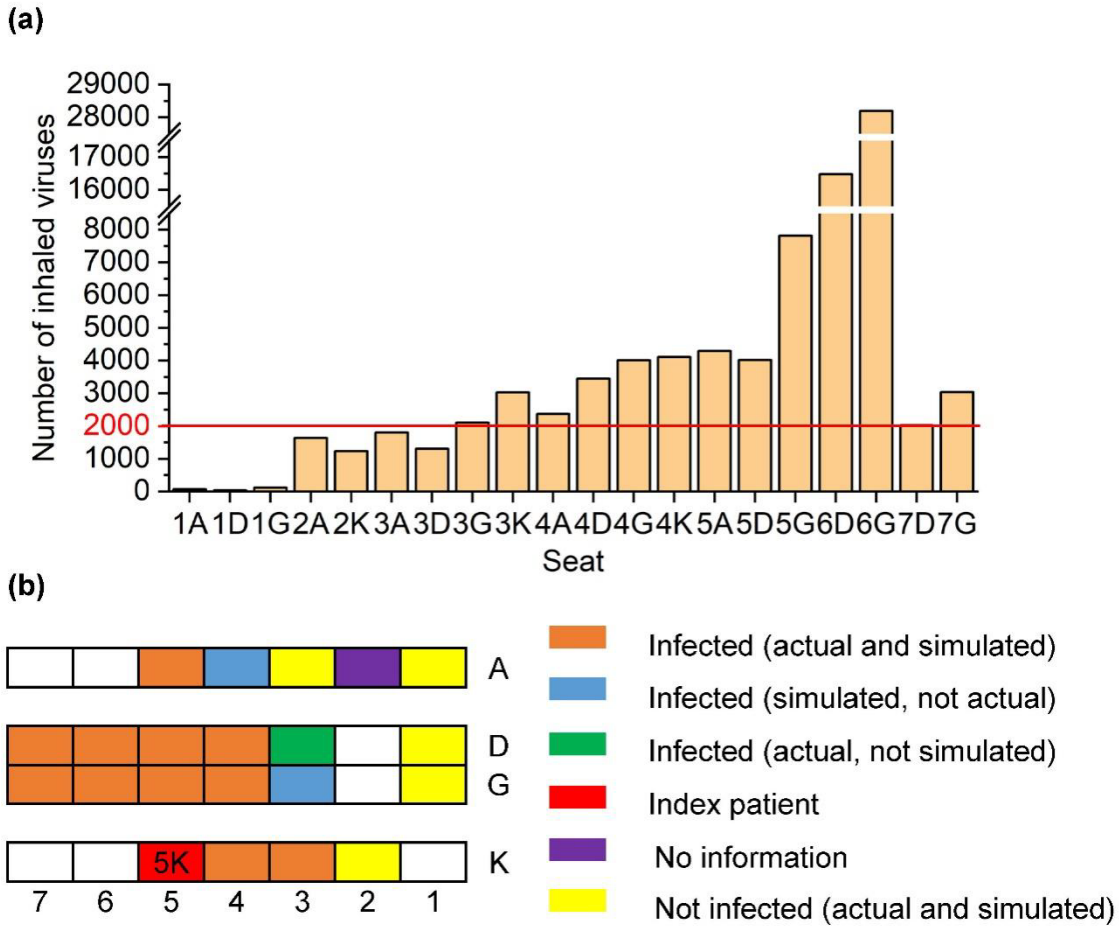

Figure 7. Simulation results: (a) number of viral copies inhaled by each passenger during the flight; (b) comparison between simulated and actual infection conditions.

4.1.4 Number of inhaled viral copies according to droplet size

It is important to know which droplet size range caused the infection in the cabin. The virus inhalation by typical passengers (2A, 2K, 5G, and 6G) during travel was calculated according to droplet size, as presented in Figure 8. It can be seen that droplet nuclei smaller than 10 μm played a major role in the infection of passengers. Actually,99% of the inhaled virus was from droplet nuclei smaller 10 μm for all susceptible passengers in the VN54 case.

Chen et al. [55] had similar finding as our study. They studied the particle size distribution of the inhaled and deposited droplets of talking and coughing. Based on their data, we further calculated the inhaled virus distributions. In their studies, 99% of the inhaled virus were from particles with nucleus diameter less than 10 μm when the distance between the patient and the susceptible person was 0.5 m and 0.9 m for talking and coughing activities, respectively.

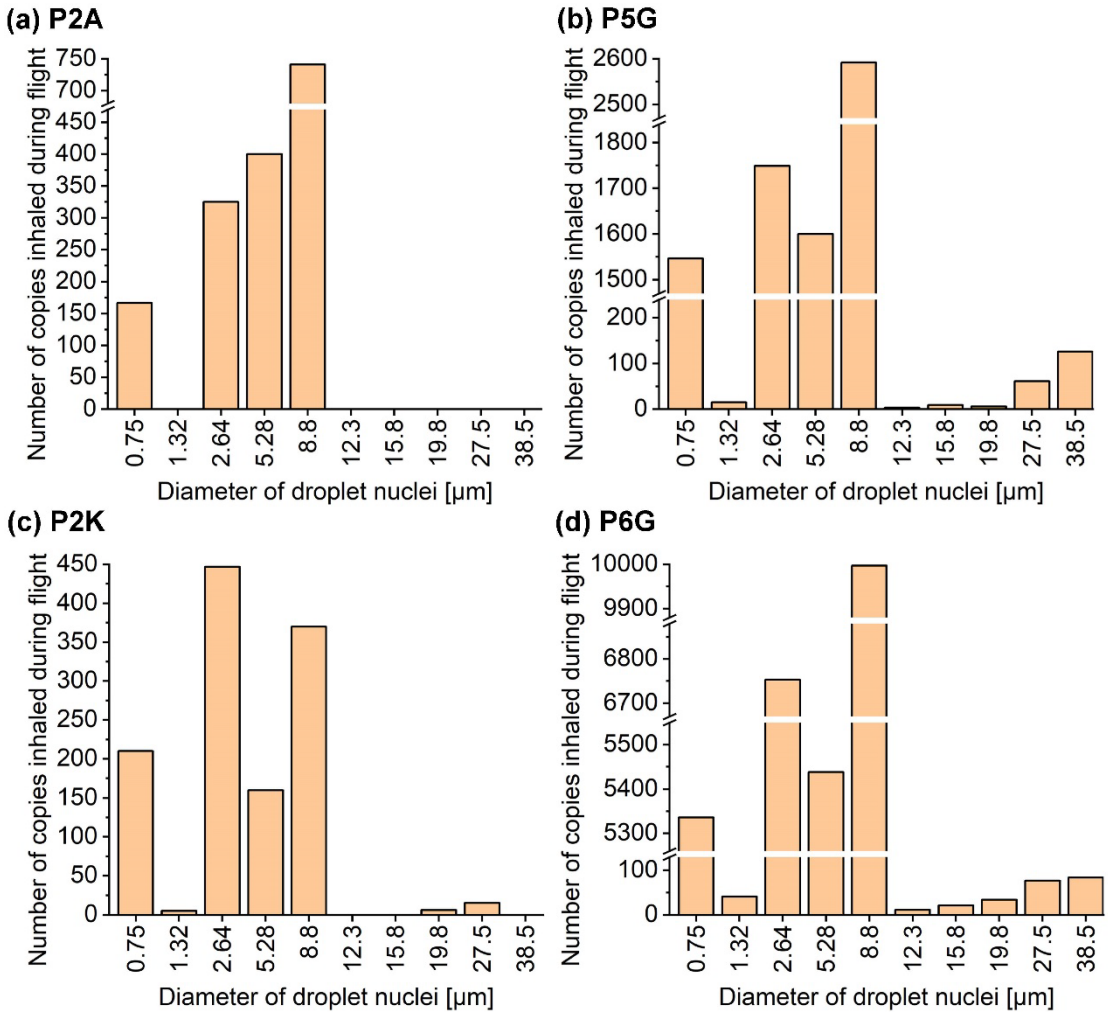

Figure 8. Inhalation of the virus according to droplet size by passengers in seats (a) 2A, (b) 5G, (c) 2K, and (d) 6G.

4.2 SARS-CoV-2 transmission during flight TR188

The second flight took off from Singapore Changi Airport at 4:50 p.m. (Beijing time, UTC+8) on January 24, 2020, and landed at 9:40 p.m. (Beijing time, UTC+8) on the same day at Hangzhou Xiaoshan Airport, China. Assuming that boarding and taxiing required a total of 40 minutes, the entire flight duration was 5 hours 30 minutes. An epidemiological investigation revealed that a total of 16 passengers were diagnosed with COVID-19 [51], but most of them were infected before boarding the airplane. Only passenger 29B was infected during the flight [51]. He sat in seat 30F for an hour and talked with his wife and son, who were in seats 31E and 31F. In close proximity to seat 30F, four confirmed patients were seated in 30E, 30F, 31J and 31K. Passenger 31K had symptoms, while passengers 30E, 30F, and 31J were asymptomatic. In addition, passengers 31K and 31J were husband and wife, whereas passengers 30E and 30D were

unrelated. According to the investigation, all the passengers were wearing masks, but passenger 30F loosened his mask while talking to his wife and son. Figure 9(a) shows the distribution of COVID-19 cases.

As in the previous case, flight TR188 was on a Boeing 787-9 aircraft. It was impractical to model and calculate the entire cabin, but many studies have found that reasonable flow and contaminant transport results can be obtained by modeling the three rows in front of and three rows behind an index patient [25,26,56,57]. In this case, with the exception of Rows 30 and 31, there were no patients in Rows 19 to 43. There were lavatories in front of Row 30, and curtains were drawn across the aisles. Therefore, this investigation simulated SARS-CoV-2 transmission from Row 30 to Row 34, as shown in Figure 9(b).

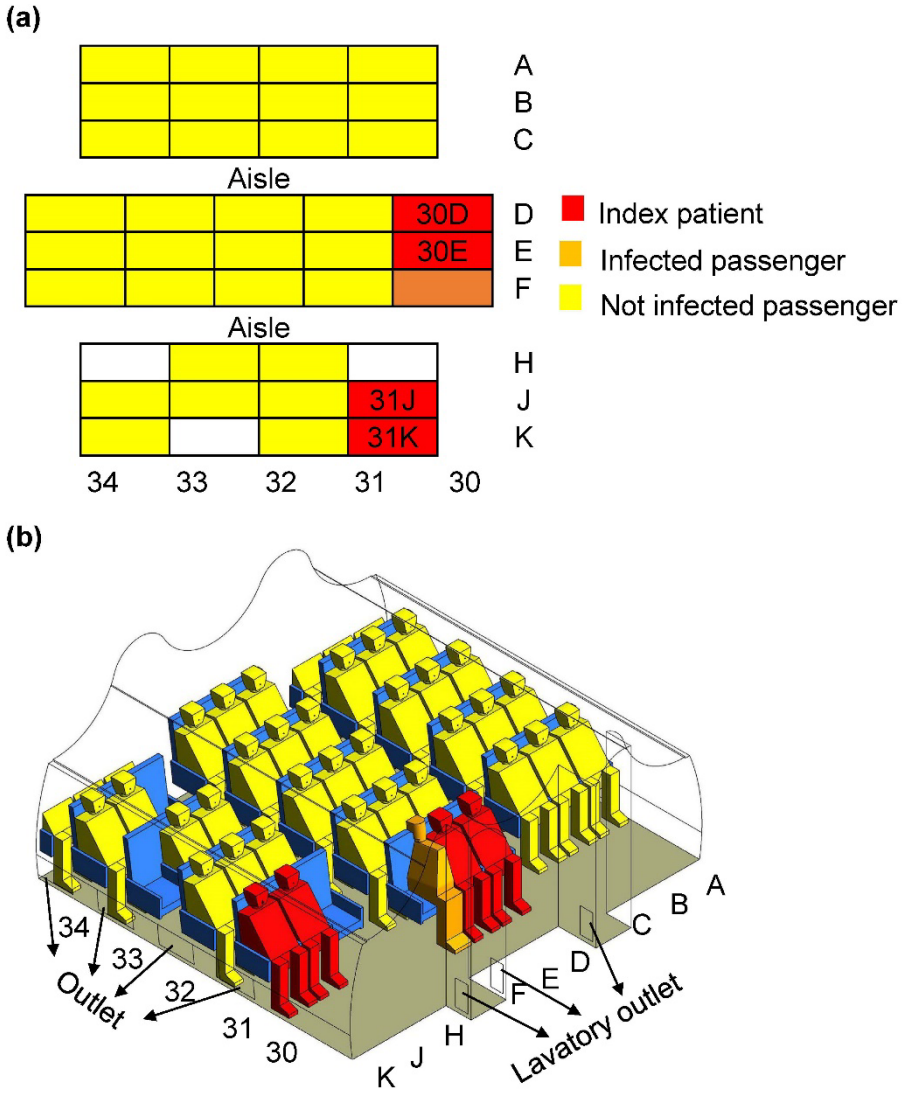

Figure 9. (a) Schematic diagram of the distribution of COVID-19 patients in Rows 30–34 of flight TR188; (b) geometric model of Boeing 787-9 economy-class cabin.

476
477 4.2.1 Particle transport
478 The airflow field of TR188 resembles that of VN54, since both flights were on
479 Boeing 787-9 aircraft, and the boundary conditions were the same. As in the VN54 flow
480 field in Figure 5, two vortices in opposite directions were formed in the TR188 cabin.
481 The transport of coughing- and breathing-generated particles during flight TR188
482 is not shown here because it resembled the transport depicted in Figure 6 for flight
483 VN54. The transport of particles expelled by possible talking activity after outward
484 filtration by masks is shown in Figure 10 in both perspective and side views, with the
485 talking between passengers 30D and 30E used as an example. Although 30E was in the
486 middle of the cabin, droplets spread to the left side of the cabin because the passenger's
487 head was turned to the left. Due to the large vortices, most of the talking-expelled
488 particles remained trapped on the left side of the cabin for a long time. In addition, when
489 released, droplets with sizes greater than 5.28 μm were all filtered by the passenger's
490 mask.

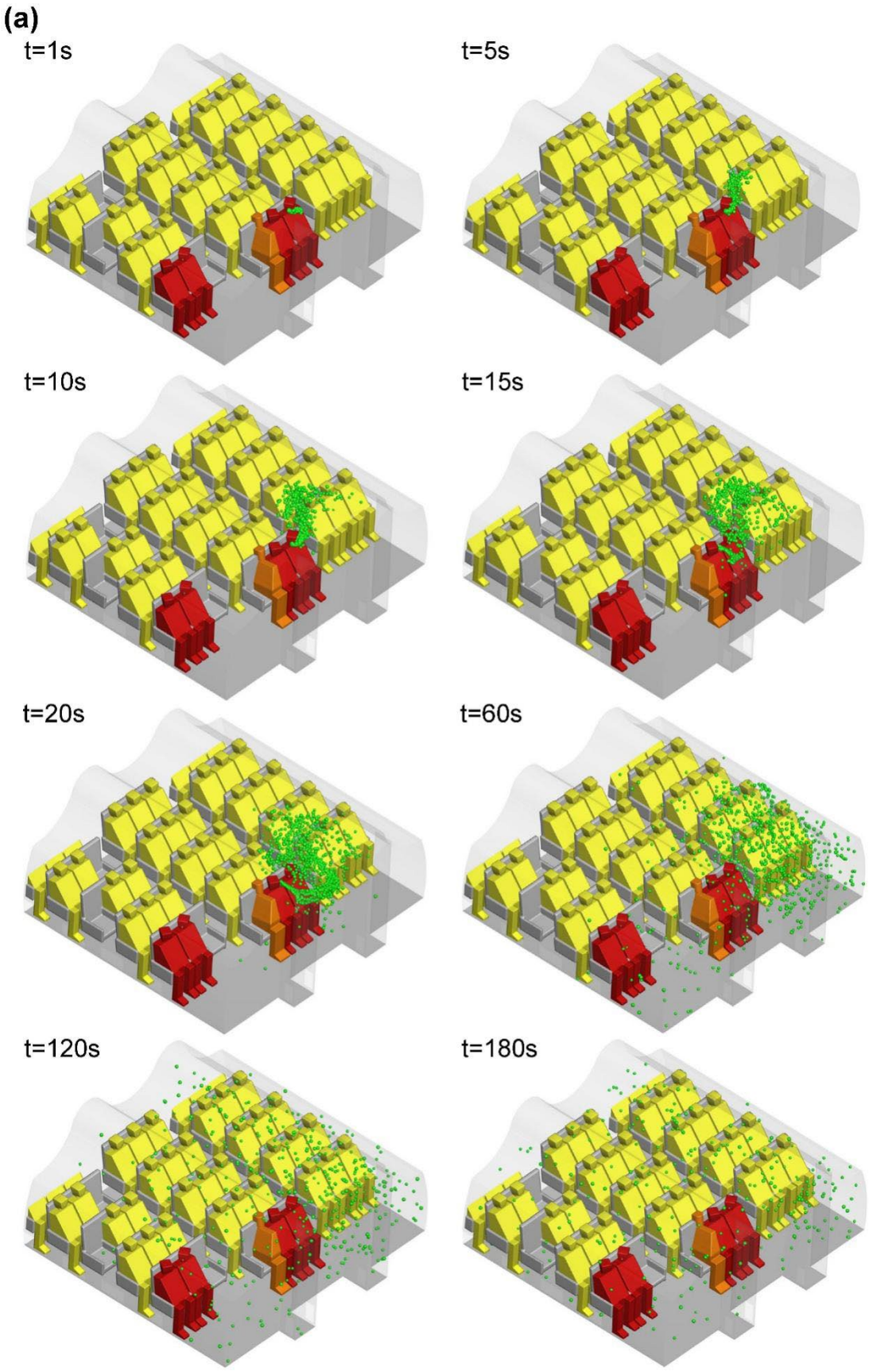
(a)
t=1s
t=5s
t=10s
t=15s
t=20s
t=60s
t=120s
t=180s

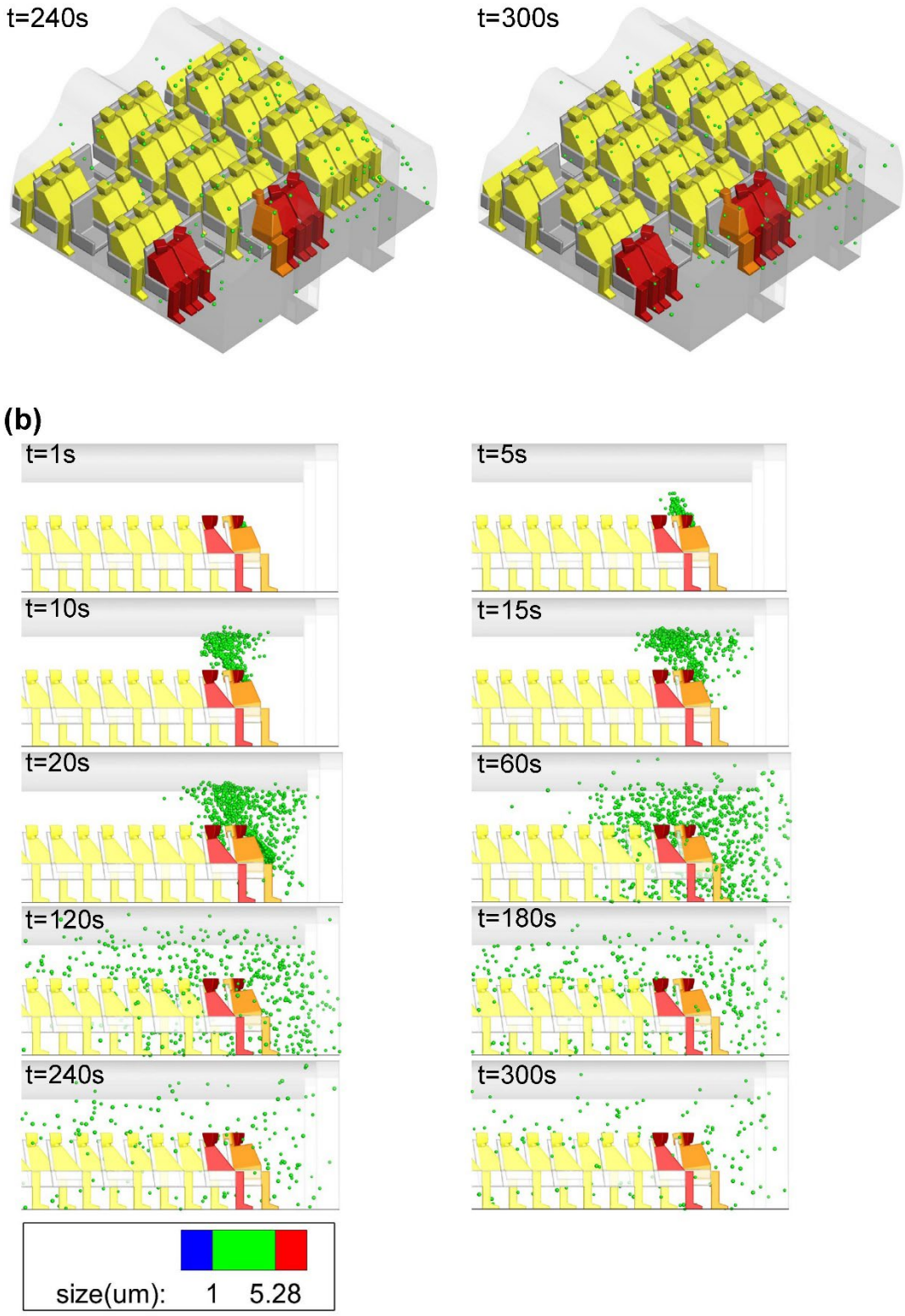

Figure 10. Temporal distributions of droplets generated due by talking between the 30D and 30E passengers in (a) perspective view and (b) side view in the TR188 case.

4.2.2 Infection risk assessment

Because no information about passengers' conversations was available for the TR188 flight, we first examined the results due to coughing and breathing by the index patients. Figure 11 shows the distribution of the number of inhaled viral copies due to coughing and breathing in the studied cabin segment of flight TR188. Passenger 30F sat in that seat for only one hour, so the calculation for him considered only one hour of exposure. The rest of the passengers stayed in their original seats throughout the flight (5 hours 30 minutes). The number of viral copies in Figure 11 did not exceed the infection limit for any of the passengers, so their conversations needed to be considered.

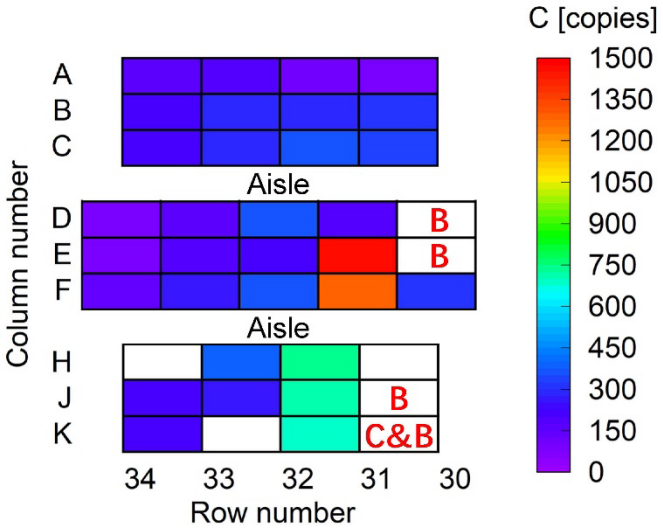

Note: C [copies] is the number of viral copies.

Figure 11. Distribution of the number of viral copies inhaled by fellow passengers due to breathing and coughing by index persons.

Two pairs of index persons, 30D & 30E and 31J & 31K, sat side by side and may have engaged in conversations that produced viral droplets. We first considered the talking time required for infection of passenger 30F during the one hour of his stay. Figure 12((a) shows the number of viral copies inhaled by 30F under different conversation durations of 30D & 30E and 31J & 31K. The talking of 31K & 31J had a larger influence on the number of inhaled viral copies than the talking of 30D & 30E. Since 30F and 31J & 31K were on the same side of the cabin, the droplets produced by 31J & 31K were trapped in the large circulation shown in Figure 5, and had a long contact time with 30F. When the conversation between 31K and 31J lasted longer than 30 minutes, the number of viral copies inhaled by 30F was greater than the tolerance limit (2000). Actually, since 31J and 31K were husband and wife, they were more likely to have conversations than strangers 30D and 30E.

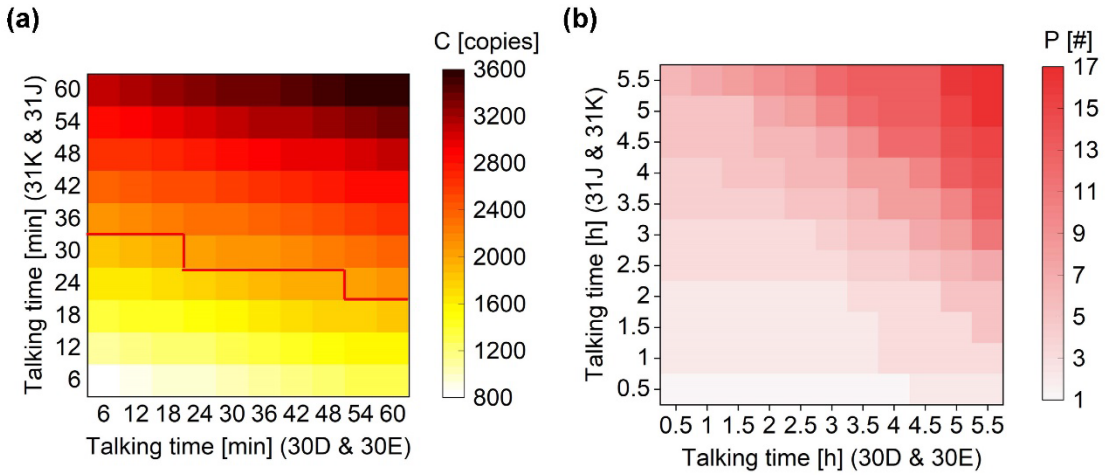

Note: C [copies] is the number of viral copies; P [#] is the number of infected passengers.

Figure 12. Influence of the conversation durations of 30D & 30E and 31J & 31K on (a) the number of viral copies inhaled by passenger 30F and (b) the number of infected passengers.

This study also examined the impact of the conversation length of index passengers on the number of infected passengers in Figure 12(b). As the length of the conversation increased, the number of infected passengers also increased. A maximum of 17 passengers might be infected if the two pairs of index persons were to have nonstop conversations throughout the duration of the flight. Reducing passenger-to-passenger communication is an effective way to control the risk of exposure. The fact that only passenger 30F was infected is an indication that the conversations were short.

5. **Discussion**

Our study used the droplet nucleus directly for the evaluation of droplet transmission and neglected the evaporation of the exhaled droplets. According to Gupta et al. [25], the evaporation of droplets with an initial diameter less than 30 μm can be ignored. According to our results, the size of the largest droplets inhaled by the passengers was 87.5 μm, and droplets larger than 87.5 μm were deposited on the walls and floor due to large inertia. Our calculations also revealed that droplets with sizes greater than 30 μm provided less than 1% of the total inhaled viral copies. Thus, it is reasonable to ignore droplet evaporation.

The estimation of the infection risk used fixed values of coughing and breathing frequencies, viral load, and infection tolerance limit. In the real world, these values depended on many factors from each individual. However, since no information was available for determining the probability of infection, our study used averaged values for tolerance limit and coughing and breathing frequencies from literature. Usually,

553 average values occurred at the highest frequency, so it was an approximation that could
554 lead to a typical result. For viral load, since the VN54 case was a super spread event
555 with very high infection rate, high viral load was assumed. Then we correctly predicted
556 84.2% of the infection, showing that the deterministic method used in this study could
557 be acceptable.
558 Our study showed that, among all the passengers, the maximum number of inhaled
559 droplets accounted for 0.114% of all exhaled droplets. The U.S. Department of
560 Transportation Command (USTRANSCOM) conducted aerosol dispersion tests in a
561 commercial aircraft cabin, and the experimental results indicated that the maximum
562 number of inhaled particles accounted for 0.3% of the total release [29]. Since the
563 percentages from the USTRANSCOM test and our simulation correspond with each
564 other, the method of directly counting the number of inhaled droplets in the nose is a
565 practical approach.
566 One important reason for the low infection rate during flight TR188 was the use
567 of masks. However, the loosening of the mask by passenger 30F increased the number
568 of viral copies that he inhaled and greatly contributed to his infection. This study also
569 investigated the effect of mask use during flight VN54 by comparing the viral copies
570 inhaled by fellow passengers for the following scenarios: no masks, only the index
571 person wearing a mask, and all passengers wearing masks. According to our analysis,
572 using masks would greatly reduce the infection risk. If just the index patient wore a
573 mask, only two passengers would be infected. If all passengers used masks for
574 protection, the number of infections would drop to one. Using masks on index
575 passengers had a better protective effect than on fellow passengers, because the inward
576 protection efficiency of masks was much lower than outward protection efficiency, as
577 shown in Table 5.
578

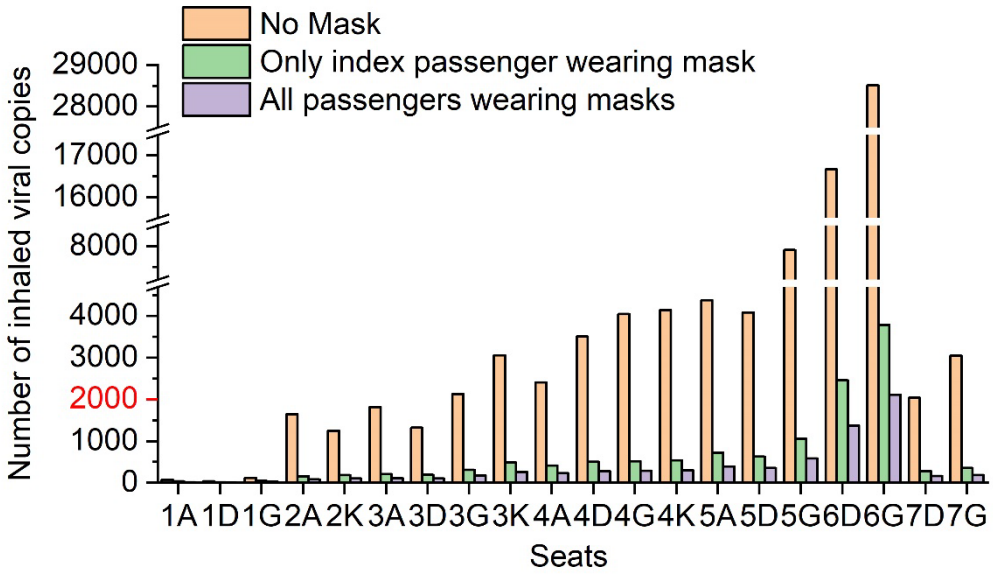

Figure 13. Number of viral copies inhaled by each passenger during the flight under different mask-wearing scenarios.

6. Conclusions

This study used CFD to numerically study the SARS-COV-2 transmission and infection process during two actual flights: VN54 (London to Hanoi) and TR188 (Singapore to Hangzhou). The generation, spread, and inhalation of respiratory droplets of different sizes produced by breathing, coughing, and talking were simulated, and the number of viral copies inhaled by fellow passengers was counted and compared with the tolerance dose to determine infection. Through the research led to the following conclusions:

1. For flight VN54, our method correctly predicted 84.2% of the infected/uninfected cases,.
2. eThe inhaled virus carried by droplet nuclei smaller than 10 μm accounted for more than 99% of the total amount of virus inhaled.
3. For the TR188 case, we found that breathing and coughing alone were not sufficient to cause infection. Therefore, we examined the influence of various conversation durations on the infection situation, and found that the index patient talking played an important role in the spread of the COVID-19.
4. Masks had positive effects on protecting passengers: The wearing of a surgical mask by the index patient would greatly reduce the number of infections, from 12 to two, and if all passengers wore surgical masks, the number of infections would be further reduced to one.

Acknowledgement

Reference

[1] Johns Hopkins University & Medicine, COVID-19 Dashboard, Johns Hopkins Coronavirus Resource Center. (n.d.). https://coronavirus.jhu.edu/map.html (accessed August 8, 2021).

[2] D. Kang, H. Choi, J.-H. Kim, J. Choi, Spatial epidemic dynamics of the COVID-19 outbreak in China, International Journal of Infectious Diseases. 94 (2020) 96–102. https://doi.org/10.1016/j.ijid.2020.03.076.

[3] N.C. Khanh, P.Q. Thai, H.-L. Quach, N.-A.H. Thi, P.C. Dinh, T.N. Duong, L.T.Q. Mai, N.D. Nghia, T.A. Tu, L.N. Quang, T.D. Quang, T.-T. Nguyen, F. Vogt, D.D. Anh, Transmission of SARS-CoV 2 During Long-Haul Flight, Emerg. Infect. Dis. 26 (2020) 2617–2624. https://doi.org/10.3201/eid2611.203299.

[4] E.M. Choi, D.K.W. Chu, P.K.C. Cheng, D.N.C. Tsang, M. Peiris, D.G. Bausch, L.L.M. Poon, D. Watson-Jones, In-Flight Transmission of SARS-CoV-2, Emerg. Infect. Dis. 26 (2020) 2713–2716. https://doi.org/10.3201/eid2611.203254.

[5] T. Swadi, J.L. Geoghegan, T. Devine, C. McElnay, X. Ren, M. Storey, S. Jefferies, J. Sherwood, E.S. FRCPath, J. Hadfield, A. Kenny, L.J. MAppSc, A.S. Ma, A. McNeill, G.E. Reynolds, K. Mouldey, L. Lowe, G. Sonder, A.J. Drummond, S. Huang, E.C. Holmes, N. French, C.R. Simpson, J. de Ligt, A case study of extended in-flight transmission of SARS- CoV-2 en route to Aotearoa New Zealand, Institute of Environmental Science and Research. New Zealand. (2020). https://doi.org/10.26091/ESRNZ.13257914.v1.

[6] L. Morawska, J.W. Tang, W. Bahnfleth, P.M. Bluyssen, A. Boerstra, G. Buonanno, J. Cao, S. Dancer, A. Floto, F. Franchimon, C. Haworth, J. Hogeling, C. Isaxon, J.L. Jimenez, J. Kurnitski, Y. Li, M. Loomans, G. Marks, L.C. Marr, L. Mazzarella, A.K. Melikov, S. Miller, D.K. Milton, W. Nazaroff, P.V. Nielsen, C. Noakes, J. Peccia, X. Querol, C. Sekhar, O. Seppänen, S. Tanabe, R. Tellier, K.W. Tham, P. Wargocki, A. Wierzbicka, M. Yao, How can airborne transmission of COVID-19 indoors be minimised?, Environment International. 142 (2020) 105832. https://doi.org/10.1016/j.envint.2020.105832.

[7] J.W. Tang, A.D. Nicolle, C.A. Klettner, J. Pantelic, L. Wang, A.B. Suhaimi, A.Y.L. Tan, G.W.X. Ong, R. Su, C. Sekhar, D.D.W. Cheong, K.W. Tham, PLOS ONE. 8 (2013) e59970. https://doi.org/10.1371/journal.pone.0059970.

[8] J.K. Gupta, C.-H. Lin, Q. Chen, Characterizing exhaled airflow from breathing and talking, Indoor Air. 20 (2010) 31–39. https://doi.org/10.1111/j.1600-0668.2009.00623.x.

[9] J.K. Gupta, C.-H. Lin, Q. Chen, Flow dynamics and characterization of a cough, Indoor Air. 19 (2009) 517–525. https://doi.org/10.1111/j.1600-0668.2009.00619.x.

[10] C. Chen, C.-H. Lin, Z. Jiang, Q. Chen, Simplified models for exhaled airflow from a cough with the mouth covered, Indoor Air. 24 (2014) 580–591.

https://doi.org/10.1111/ina.12109.
[11] P. Höppe, Temperatures of expired air under varying climatic conditions, Int J Biometeorol. 25 (1981) 127–132. https://doi.org/10.1007/BF02184460.
[12] M. Nicas, W.W. Nazaroff, A. Hubbard, Toward Understanding the Risk of Secondary Airborne Infection: Emission of Respirable Pathogens, Journal of Occupational and Environmental Hygiene. 2 (2005) 143–154. https://doi.org/10.1080/15459620590918466.
[13] P. Fabian, J.J. McDevitt, W.H. DeHaan, R.O.P. Fung, B.J. Cowling, K.H. Chan, G.M. Leung, D.K. Milton, Influenza Virus in Human Exhaled Breath: An Observational Study, PLoS ONE. 3 (2008) e2691. https://doi.org/10.1371/journal.pone.0002691.
[14] S. Yang, G.W.M. Lee, C.-M. Chen, C.-C. Wu, K.-P. Yu, The Size and Concentration of Droplets Generated by Coughing in Human Subjects, Journal of Aerosol Medicine. 20 (2007) 484–494. https://doi.org/10.1089/jam.2007.0610.
[15] C.Y.H. Chao, M.P. Wan, L. Morawska, G.R. Johnson, Z.D. Ristovski, M. Hargreaves, K. Mengersen, S. Corbett, Y. Li, X. Xie, D. Katoshevski, Characterization of expiration air jets and droplet size distributions immediately at the mouth opening, Journal of Aerosol Science. 40 (2009) 122–133. https://doi.org/10.1016/j.jaerosci.2008.10.003.
[16] G. Zayas, M.C. Chiang, E. Wong, F. MacDonald, C.F. Lange, A. Senthilselvan, M. King, Cough aerosol in healthy participants: fundamental knowledge to optimize droplet-spread infectious respiratory disease management, BMC Pulm Med. 12 (2012) 11. https://doi.org/10.1186/1471-2466-12-11.
[17] J.P. Duguid, The size and the duration of air-carriage of respiratory droplets and droplet-nuclei, Epidemiology & Infection. 44 (1946) 471–479. https://doi.org/10.1017/S0022172400019288.
[18] Z.Y. Han, W.G. Weng, Q.Y. Huang, Characterizations of particle size distribution of the droplets exhaled by sneeze, Journal of The Royal Society Interface. 10 (2013) 20130560. https://doi.org/10.1098/rsif.2013.0560.
[19] Y. Yan, X. Li, J. Tu, Thermal effect of human body on cough droplets evaporation and dispersion in an enclosed space, Building and Environment. 148 (2019) 96–106. https://doi.org/10.1016/j.buildenv.2018.10.039.
[20] Y. Feng, T. Marchal, T. Sperry, H. Yi, Influence of wind and relative humidity on the social distancing effectiveness to prevent COVID-19 airborne transmission: A numerical study, Journal of Aerosol Science. 147 (2020) 105585. https://doi.org/10.1016/j.jaerosci.2020.105585.
[21] Y. Yan, X. Li, L. Yang, P. Yan, J. Tu, Evaluation of cough-jet effects on the transport characteristics of respiratory-induced contaminants in airline passengers' local environments, Building and Environment. 183 (2020) 107206. https://doi.org/10.1016/j.buildenv.2020.107206.
[22] K. Talaat, M. Abuhegazy, O.A. Mahfoze, O. Anderoglu, S.V. Poroseva, Simulation of aerosol transmission on a Boeing 737 airplane with intervention

687 measures for COVID-19 mitigation, Physics of Fluids. 33 (2021) 033312.
688 https://doi.org/10.1063/5.0044720.
689 [23] Y. Liu, Z. Ning, Y. Chen, M. Guo, Y. Liu, N.K. Gali, L. Sun, Y. Duan, J. Cai, D.
690 Westerdahl, X. Liu, K. Xu, K. Ho, H. Kan, Q. Fu, K. Lan, Aerodynamic analysis
691 of SARS-CoV-2 in two Wuhan hospitals, Nature. 582 (2020) 557–560.
692 https://doi.org/10.1038/s41586-020-2271-3.
693 [24] J.K. Gupta, C.-H. Lin, Q. Chen, Risk assessment of airborne infectious diseases
694 in aircraft cabins, Indoor Air. 22 (2012) 388–395. https://doi.org/10.1111/j.1600-
695 0668.2012.00773.x.
696 [25] J.K. Gupta, C.-H. Lin, Q. Chen, Transport of expiratory droplets in an aircraft
697 cabin, Indoor Air. 21 (2011) 3–11. https://doi.org/10.1111/j.1600-
698 0668.2010.00676.x.
699 [26] Y. Yan, X. Li, Y. Shang, J. Tu, Evaluation of airborne disease infection risks in an
700 airliner cabin using the Lagrangian-based Wells-Riley approach, Building and
701 Environment. 121 (2017) 79–92. https://doi.org/10.1016/j.buildenv.2017.05.013.
702 [27] J. Wei, Y. Li, Enhanced spread of expiratory droplets by turbulence in a cough jet,
703 Building and Environment. 93 (2015) 86–96.
704 https://doi.org/10.1016/j.buildenv.2015.06.018.
705 [28] X. Xie, Y. Li, A.T.Y. Chwang, P.L. Ho, W.H. Seto, How far droplets can move in
706 indoor environments - revisiting the Wells evaporation-falling curve, Indoor Air.
707 17 (2007) 211–225. https://doi.org/10.1111/j.1600-0668.2007.00469.x.
708 [29] D. Silcott, S. Kinahan, J. Santarpia, B. Silcott, P. Silcott, B. Silcott, S. Distelhorst,
709 V. Herrera, D. Rivera, K. Crown, TRANSCOM/AMC commercial aircraft cabin
710 aerosol dispersion tests, National Strategic Research Institute Lincoln United
711 States, 2020.
712 [30] X. Li, T. (Tim) Zhang, M. Fan, M. Liu, D. Chang, Z. (Daniel) Wei, C.-H. Lin, S.
713 Ji, J. Liu, S. Shen, Z. Long, Experimental evaluation of particle exposure at
714 different seats in a single-aisle aircraft cabin, Building and Environment. 202
715 (2021) 108049. https://doi.org/10.1016/j.buildenv.2021.108049.
716 [31] R. You, W. Liu, J. Chen, C.-H. Lin, D. Wei, Q. Chen, Predicting airflow
717 distribution and contaminant transport in aircraft cabins with a simplified gasper
718 model, Journal of Building Performance Simulation. 9 (2016) 699–708.
719 https://doi.org/10.1080/19401493.2016.1196730.
720 [32] Z. Zhang, W. Zhang, Z.J. Zhai, Q.Y. Chen, Evaluation of Various Turbulence
721 Models in Predicting Airflow and Turbulence in Enclosed Environments by CFD:
722 Part 2—Comparison with Experimental Data from Literature, HVAC&R Research.
723 13 (2007) 871–886. https://doi.org/10.1080/10789669.2007.10391460.
724 [33] I. Ansys, Inc, ANSYS FLUENT theory guide, Canonsburg, Pa. 794 (2011).
725 [34] Z. Zhang, Q. Chen, Comparison of the Eulerian and Lagrangian methods for
726 predicting particle transport in enclosed spaces, Atmospheric Environment. 41
727 (2007) 5236–5248. https://doi.org/10.1016/j.atmosenv.2006.05.086.
728 [35] C. Chen, B. Zhao, Some questions on dispersion of human exhaled droplets in

729 ventilation room: answers from numerical investigation, Indoor Air. 20 (2010) 95–
730 111. https://doi.org/10.1111/j.1600-0668.2009.00626.x.
731 [36] M.D. Allen, O.G. Raabe, Slip Correction Measurements of Spherical Solid
732 Aerosol Particles in an Improved Millikan Apparatus, Aerosol Science and
733 Technology. 4 (1985) 269–286. https://doi.org/10.1080/02786828508959055.
734 [37] S.A.J. Morsi, A.J. Alexander, An investigation of particle trajectories in two-phase
735 flow systems, Journal of Fluid Mechanics. 55 (1972) 193–208.
736 [38] Centers for Disease Control and Prevention, Coronavirus Disease 2019 (COVID-
737 19) – Symptoms, Centers for Disease Control and Prevention. (2021).
738 https://www.cdc.gov/coronavirus/2019-ncov/symptoms-testing/symptoms.html
739 (accessed August 27, 2021).
740 [39] G.R. Johnson, L. Morawska, Z.D. Ristovski, M. Hargreaves, K. Mengersen,
741 C.Y.H. Chao, M.P. Wan, Y. Li, X. Xie, D. Katoshevski, S. Corbett, Modality of
742 human expired aerosol size distributions, Journal of Aerosol Science. 42 (2011)
743 839–851. https://doi.org/10.1016/j.jaerosci.2011.07.009.
744 [40] Y. Pan, D. Zhang, P. Yang, L.L.M. Poon, Q. Wang, Viral load of SARS-CoV-2 in
745 clinical samples, The Lancet Infectious Diseases. 20 (2020) 411–412.
746 https://doi.org/10.1016/S1473-3099(20)30113-4.
747 [41] K.K.-W. To, O.T.-Y. Tsang, C.C.-Y. Yip, K.-H. Chan, T.-C. Wu, J.M.-C. Chan, W.-
748 S. Leung, T.S.-H. Chik, C.Y.-C. Choi, D.H. Kandamby, D.C. Lung, A.R. Tam,
749 R.W.-S. Poon, A.Y.-F. Fung, I.F.-N. Hung, V.C.-C. Cheng, J.F.-W. Chan, K.-Y.
750 Yuen, Consistent Detection of 2019 Novel Coronavirus in Saliva, Clinical
751 Infectious Diseases. 71 (2020) 841–843. https://doi.org/10.1093/cid/ciaa149.
752 [42] W.G. Lindsley, F.M. Blachere, R.E. Thewlis, A. Vishnu, K.A. Davis, G. Cao, J.E.
753 Palmer, K.E. Clark, M.A. Fisher, R. Khakoo, D.H. Beezhold, Measurements of
754 Airborne Influenza Virus in Aerosol Particles from Human Coughs, PLOS ONE.
755 5 (2010) e15100. https://doi.org/10.1371/journal.pone.0015100.
756 [43] K.P. Fennelly, Particle sizes of infectious aerosols: implications for infection
757 control, The Lancet Respiratory Medicine. 8 (2020) 914–924.
758 https://doi.org/10.1016/S2213-2600(20)30323-4.
759 [44] J. Pan, C. Harb, W. Leng, L.C. Marr, Inward and outward effectiveness of cloth
760 masks, a surgical mask, and a face shield, Aerosol Science and Technology. 55
761 (2021) 718–733. https://doi.org/10.1080/02786826.2021.1890687.
762 [45] International Commission on Radiological Protection (ICRP), Human respiratory
763 tract model for radiological protection. A report of a Task Group of the
764 International Commission on Radiological Protection, Ann ICRP. 24 (1994) 1–
765 482.
766 [46] J.K. Gupta, C.-H. Lin, Q. Chen, Inhalation of expiratory droplets in aircraft cabins,
767 Indoor Air. 21 (2011) 341–350. https://doi.org/10.1111/j.1600-0668.2011.00709.x.
768 [47] M.P. Wan, C.Y.H. Chao, Transport Characteristics of Expiratory Droplets and
769 Droplet Nuclei in Indoor Environments With Different Ventilation Airflow
770 Patterns, Journal of Biomechanical Engineering. 129 (2006) 341–353.

https://doi.org/10.1115/1.2720911.
[48] M. Prentiss, A. Chu, K.K. Berggren, Superspreading Events Without Superspreaders: Using High Attack Rate Events to Estimate N º for Airborne Transmission of COVID-19, Epidemiology, 2020. https://doi.org/10.1101/2020.10.21.20216895.
[49] C.-H.- Lin, K.H. Dunn, R.H. Horstman, J.L. Topmiller, M.F. Ahlers, J.S. Bennett, L.M. Sedgwick, S. Wirogo, Numerical Simulation of Airflow and Airborne Pathogen Transport in Aircraft Cabins--Part I: Numerical Simulation of the Flow Field., ASHRAE Transactions. 111 (2005).
[50] M. Liu, D. Chang, J. Liu, S. Ji, C.-H. Lin, D. Wei, Z. Long, T. Zhang, X. Shen, Q. Cao, X. Li, X. Zeng, H. Li, Experimental investigation of air distribution in an airliner cabin mockup with displacement ventilation, Building and Environment. 191 (2021) 107577. https://doi.org/10.1016/j.buildenv.2020.107577.
[51] J. Chen, H. He, W. Cheng, Y. Liu, Z. Sun, C. Chai, Q. Kong, W. Sun, J. Zhang, S. Guo, X. Shi, J. Wang, E. Chen, Z. Chen, Potential transmission of SARS-CoV-2 on a flight from Singapore to Hangzhou, China: An epidemiological investigation, Travel Medicine and Infectious Disease. 36 (2020) 101816. https://doi.org/10.1016/j.tmaid.2020.101816.
[52] A.P. Sunjaya, C. Jenkins, Rationale for universal face masks in public against COVID-19, Respirology. 25 (2020) 678–679. https://doi.org/10.1111/resp.13834.
[53] H. Elachola, S.H. Ebrahim, E. Gozzer, COVID-19: Facemask use prevalence in international airports in Asia, Europe and the Americas, March 2020, Travel Medicine and Infectious Disease. 35 (2020) 101637. https://doi.org/10.1016/j.tmaid.2020.101637.
[54] M. Keshtkar-Jahromi, M. Sulkowski, K. Holakouie-Naieni, Public Masking: An Urgent Need to Revise Global Policies to Protect against COVID-19, The American Journal of Tropical Medicine and Hygiene. 102 (2020) 1160–1161. https://doi.org/10.4269/ajtmh.20-0305.
[55] W. Chen, N. Zhang, J. Wei, H.-L. Yen, Y. Li, Short-range airborne route dominates exposure of respiratory infection during close contact, Building and Environment. 176 (2020) 106859. https://doi.org/10.1016/j.buildenv.2020.106859.
[56] R. You, C.-H. Lin, D. Wei, Q. Chen, Evaluating the commercial airliner cabin environment with different air distribution systems, Indoor Air. 29 (2019) 840–853. https://doi.org/10.1111/ina.12578.
[57] N.P. Gao, J.L. Niu, Personalized Ventilation for Commercial Aircraft Cabins, Journal of Aircraft. 45 (2008) 508–512. https://doi.org/10.2514/1.30272.